

# Methane hydrogenation and confirmation of CH<sub>x</sub> intermediate species on NaY encapsulated cobalt clusters and Co/SiO<sub>2</sub> catalysts: EXAFS, FTIR, UV characterization and catalytic performances

Guo-Cheng Shen<sup>a,b\*</sup> and Masaru Ichikawa<sup>a</sup>

<sup>a</sup> Catalysis Research Center, Hokkaido University, Sapporo 060, Japan

<sup>b</sup> Department of Chemistry, University of Toronto, 80 St. George Street, Toronto, Ontario, M5S 3H6 Canada

The adsorption of Co<sub>2</sub>(CO)<sub>8</sub> onto dehydrated NaY powder under an N<sub>2</sub> atmosphere predominantly yielded supported Co<sub>4</sub>(CO)<sub>12</sub>. The molecular cobalt carbonyl clusters and their decarbonylated products have been structurally characterized by *in situ* IR, extended X-ray absorption fine structure (EXAFS) and diffuse reflectance spectroscopies. The IR spectrum assigned to the species Co<sub>4</sub>(CO)<sub>12</sub>/NaY is shifted significantly from that observed for externally supported analogues on NaY and for this cluster in solution, which indicates that the cobalt carbonyl clusters occurring on the NaY are similar to those occurring in weakly basic solution. EXAFS coordination numbers (*N*) show that the successively decarbonylated samples maintain small cluster sizes, which depend on the temperature-programmed oxidation of the precursor. Methane hydrogenation was carried out on intrazeolitic cobalt clusters using a two-step process. It showed a relatively higher activity and selectivity to C<sub>2+</sub> hydrocarbons in comparison with Co/SiO<sub>2</sub> catalysts. On the basis of IR ( $\nu_{C-H}$  2960, 2880 cm<sup>-1</sup> and  $\delta_{C-H}$  1520, 1393 cm<sup>-1</sup>) spectroscopy, mass spectrometry and reaction studies, one can conclude that CH<sub>x</sub> (*x* = 0, 1 or 2) surface carbonaceous species were generated by CH<sub>4</sub> dissociation on the activated cobalt catalyst; the CH<sub>2</sub> species was quite reactive, and propagated higher hydrocarbons.

Oxidation coupling of methane has been developed during the last decade.<sup>1–5</sup> Numerous basic metal oxides, mixed-metal oxides and doped metal oxides have been observed to be active catalysts, but co-reactants of oxygen/nitrous oxide and high temperature are necessary in this reaction procedure. These create a reaction environment conducive to deep oxidation of CH<sub>4</sub> and higher hydrocarbons to CO and CO<sub>2</sub>. Recently, Yang *et al.*<sup>6</sup> reported the synthesis of benzene on a Ni(111) surface by collision induced chemisorption of methane using molecular beam techniques under ultrahigh vacuum (UHV), and subsequent heating. Koerts and Van Santen<sup>7</sup> stimulated much interest with their proposal that methane can be converted into ethane and propane in a two-step procedure by thermal dissociation of methane on a supported metal catalyst, followed by hydrogenating the surface species deposited on the catalyst. In these papers, the adsorbed surface species seem to be key factors, which result in different kinds of hydrocarbon formation. In this regard, a high metallic surface area per unit mass is necessary for the chemisorption of methane and subsequent hydrogenation.

The well defined channel, pore microstructure, the large internal surface area and the high thermal stability of zeolites make them attractive supports for the preparation of transition-metal catalysts with large metallic surface areas. During the last decade, carbonyl clusters of Ru,<sup>8</sup> Rh,<sup>9</sup> Rd,<sup>10</sup> Ir<sup>11</sup> and Pt<sup>12</sup> have been prepared in the cages of zeolites, by ‘ship-in-a-bottle’ synthesis techniques. The activation of metal carbonyl clusters for methane conversion usually requires their decarbonylation, to give nearly structurally uniform materials that offer the prospect of being size/shape selective catalysts.<sup>13–15</sup> However, during the decarbonylation, the metal often migrates out of the zeolite pores to form crystallites on the external surface.<sup>16</sup> Preparation of metal carbonyl clusters with uniform nuclearities in zeolites has not been well demonstrated and decarbonylated metal clusters, as yet, are not well characterized.

This article reports the following: (i) intrazeolitic cobalt carbonyl clusters and their decarbonylated products are characterized by IR, EXAFS and diffuse reflectance spectroscopies

and NO chemisorption; (ii) methane hydrogenation is performed on NaY-encapsulated cobalt and Co/SiO<sub>2</sub> catalysts; (iii) the reactive intermediates are identified by IR and MS spectra.

## Experimental

### Sample preparation

An NaY zeolite-supported cobalt sample (10 wt.% Co loading) was prepared by spontaneous monolayer dispersion of Co<sub>2</sub>(CO)<sub>8</sub> (Strem Chemical, stabilized with 5–10% hexane) with NaY zeolite powder (HSZ-320NAA, Lot no. D1-9915, Si/Al = 2.8, surface area 910 m<sup>2</sup> g<sup>-1</sup>).<sup>17</sup> The NaY zeolite powder was dehydrated by evacuation at 623 K for 2 h, and then was mixed mechanically with Co<sub>2</sub>(CO)<sub>8</sub> under an N<sub>2</sub> atmosphere at 300 K, followed by 1 h ageing at 300 K, to give the brown sample, denoted as the precursor of the cobalt catalyst.

Co/SiO<sub>2</sub> (10 wt.% Co loading) was prepared by impregnation of silica (Aerosil 300, surface area 300 m<sup>2</sup> g<sup>-1</sup>, mesh 100) with a solution of Co(NO<sub>3</sub>)<sub>2</sub> · 6H<sub>2</sub>O. After drying, the sample was calcined at 673 K for 2 h, and was then reduced at 673 K for 10 h under H<sub>2</sub> flow, to give the Co/SiO<sub>2</sub> catalyst.

The concentration of Co in the samples was determined by using an inductively coupled plasma (ICP) atomic emission spectrometer. Attempts to extract organometallic species from the NaY supported samples were carried out with methanol.

### Characterization of samples

**IR spectroscopy.** *In situ* IR spectra of the samples were recorded with a Shimadzu FTIR 4200 spectrometer with 20–100 co-added scans at 2 cm<sup>-1</sup> resolution. The precursor was pressed into a self-supporting wafer (8 mg cm<sup>-2</sup>) in an N<sub>2</sub> atmosphere box and mounted in a quartz IR cell with CaF<sub>2</sub> windows that connected to a vacuum-closed circulating Pyrex-glass line (10<sup>-5</sup> Torr). The IR cell was equipped with an electric heater and a liquid-N<sub>2</sub> reservoir for high- and low-temperature measurements. Before use, all gases were passed through traps to remove water and/or oxygen.

**EXAFS spectroscopy.** EXAFS measurements were carried out at the Photon Factory in the National Laboratory for High Energy Physics (KEF-PF) using synchrotron radiation with an electron energy of 2.5 GeV at currents of 200–350 mA. The amount of sample in a wafer was calculated at the Co K absorption edge, and the sample wafers were stored in specially designed Pyrex-glass cells with kapton film windows (50 nm thick). The spectra at the Co K edge (7.7 keV) were measured at 296 K under vacuum using a Si(111) double crystal monochromator. The reference samples used were crystalline  $\text{Co}_4(\text{CO})_{12}$ ,  $\text{Co}_3\text{O}_4$  and Co foil.

**EXAFS data analysis.** The EXAFS data were extracted from the measured absorption spectra by standard methods.<sup>18</sup> The normalization was done by dividing the absorption intensities by the height of the absorption edge and subtracting the background using cubic spline routines. The final EXAFS function was obtained by averaging the individual background-subtracted and normalized EXAFS data (two scans for each sample). The main contributions to the spectra were isolated by inverse Fourier transformation of the final EXAFS function over a selected range in  $r$ -space. The analysis was performed on these Fourier-filtered data. The parameters characterizing high- $Z(\text{Co})$  and low- $Z(\text{C}, \text{O})$  contributions were reliably determined by multiple-shell fitting in  $k$  space ( $k$  is the wavevector) and  $r$  space ( $r$  is the distance from the absorbing atom) with application of  $K^2$  and  $K^3$  weighting of the Fourier transform. The accuracy and limitation of parameters were considered as:  $0.02 < \sigma < 0.08$  and  $-10 < \Delta E_0 < 10$ , as well as the (calculated EXAFS contributions – experimental EXAFS contributions)/calculated EXAFS contributions of  $R$  factor  $< 15\%$  for optimized coordination numbers ( $N$ ) and bond lengths.<sup>19</sup> The difference file technique with phase- and amplitude-corrected Fourier transforms was applied to further optimize the fit.<sup>19</sup>

**Powder X-ray diffraction (PXRD) and diffuse reflectance.** The PXRD measurement was carried out using a MAC Science diffractometer with Cu- $K\alpha$  radiation ( $\lambda = 1.5418 \text{ \AA}$ ). Diffuse reflectance spectra were recorded on a Shimadzu UV-2200 Series spectrometer with a photomultiplier detector.  $\text{BaSO}_4$  was used as a reference. The samples were stored in Pyrex-glass cells with Heraeus Amersil quartz windows. After treatment, samples were measured at room temperature.

### Methane hydrogenation

After reduction, the cobalt catalyst with adsorbed  $\text{H}_2$  was flushed with He at 300 K for 30 min. The temperature of the reaction procedure was raised to 723 K under flowing He, and then switched to a pulsed gas containing dilute  $\text{CH}_4$  by He. After methane dissociation, the cobalt catalyst was quickly cooled to room temperature (r.t.) under He flowing to avoid ageing of the surface carbonaceous species deposited on the cobalt catalyst. The surface carbonaceous species were subsequently hydrogenated in an  $\text{H}_2$  flow of  $20 \text{ cm}^{-3} \text{ STP min}^{-1}$  from 300 to 673 K. Before entering the catalyst bed, the gases (He,  $\text{CH}_4$  and  $\text{H}_2$ ) were purified with manganese oxide and molecular sieves. The effluent gases from the reactor were stored in the loops and were determined afterwards by Shimadzu GC-8A gas chromatography with a flame ionization detector.

## Results

### Characterization of NaY-supported cobalt clusters

**Precursor characterization by IR spectroscopy and powder X-ray diffraction.** The sample (10 wt.% Co loading) was characterized by PXRD. The pattern shows reflections at  $2\theta = 11.46, 16.64, 22.9, 29.78, 32.22, 32.80, 43.66$  and  $44.52^\circ$  [Fig. 1(a)], ascribed to crystalline  $\text{Co}_2(\text{CO})_8$ . In Fig. 1(b), these reflections completely disappeared, leaving only the

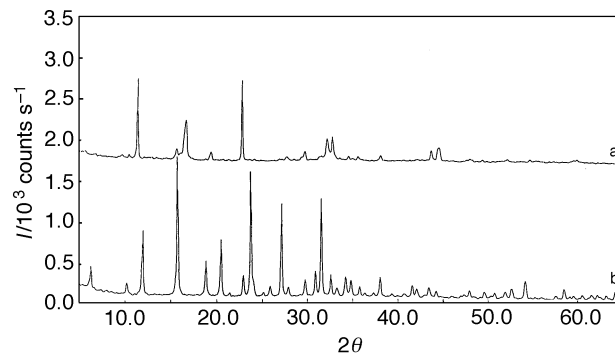


**Fig. 1** PXRD patterns of (a) crystalline  $\text{Co}_2(\text{CO})_8$  and (b)  $\text{Co}_2(\text{CO})_8$  mechanically mixed with NaY at 298 K under an  $\text{N}_2$  atmosphere

PXRD peaks for NaY. The dark-red  $\text{Co}_2(\text{CO})_8$  changed colour to brown in the precursor. This suggests that gaseous  $\text{Co}_2(\text{CO})_8$  is highly dispersed on the NaY framework, similar to what has been reported previously for  $\text{CuCl}_2/\text{NaY}$ <sup>20</sup> and  $\text{AuCl}_3/\text{NaY}$ .<sup>21</sup> Fig. 2(a) shows the IR spectrum of the precursor. The bands at  $2121\text{w}$ ,  $2078\text{s}$ ,  $2053$  (sh) and  $1816\text{m}$   $\text{cm}^{-1}$  closely resembled those of  $\text{Co}_4(\text{CO})_{12}$  in pentane solution [ $2060\text{s}$ ,  $2035$  (sh),  $1870\text{m}$   $\text{cm}^{-1}$ ; Fig. 2(c)] which has three edge-bridging CO and nine terminal CO ligands.<sup>22</sup>  $\text{Co}_4(\text{CO})_{12}$  appears to be formed from  $\text{Co}_2(\text{CO})_8$  on NaY zeolite. On other hand, the weak band at  $1901 \text{ cm}^{-1}$  in Fig. 2(a) can be assigned directly to  $\text{Co}(\text{CO})_4^-$  species.<sup>23</sup> Some CO (g) was released as shown by the band at  $2153 \text{ cm}^{-1}$  in Fig. 2(a). The relative abundances of  $\text{Co}_4(\text{CO})_{12}$  and  $\text{Co}(\text{CO})_4^-$  species of the precursor were calculated from the areas of the two  $\text{CO}_t$  bands in  $\text{Co}_4(\text{CO})_{12}$  and the  $\text{CO}_t$  in  $\text{Co}(\text{CO})_4^-$  species, where

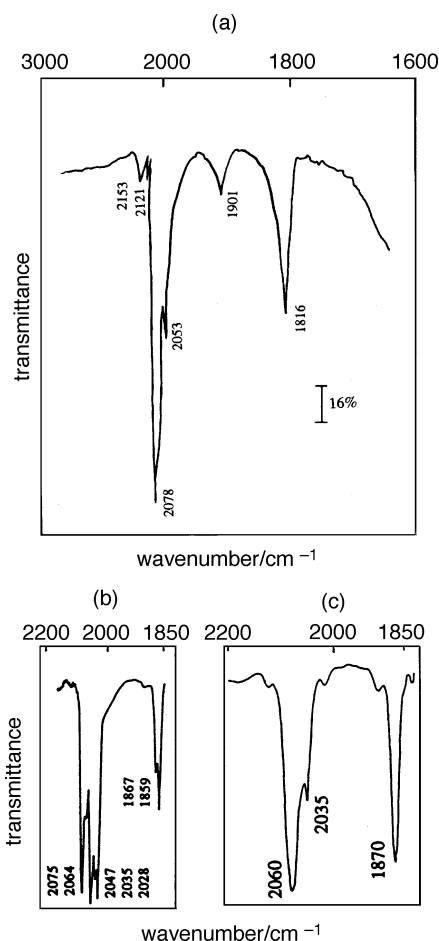


**Fig. 2** IR spectra obtained for (a)  $\text{Co}_2(\text{CO})_8$  adsorbed on dehydrated NaY powder under  $\text{N}_2$  atmosphere, for (b)  $\text{Co}_2(\text{CO})_8$  in pentane solution and for (c)  $\text{Co}_4(\text{CO})_{12}$  in pentane solution

equal absorption coefficients of  $\text{CO}_i$  for  $\text{Co}_4(\text{CO})_{12}$  and  $\text{Co}(\text{CO})_4^-$  species were assumed; the calculated abundance is 90% for  $\text{Co}_4(\text{CO})_{12}$  and 10% for  $\text{Co}(\text{CO})_4^-$ .

The  $\text{Co}_4(\text{CO})_{12}$  in the precursor is identified by principal  $\nu_{\text{CO}}$  bands at 2121w, 2078s, 2053 (sh) and 1816m  $\text{cm}^{-1}$ . The 2078 and 2053  $\text{cm}^{-1}$  bands are assigned to the symmetric and asymmetric stretching of the two CO ligands bound to each Co atom of three out of four Co atoms in  $\text{Co}_4(\text{CO})_{12}$ ; the 2121, 2078 and 2053  $\text{cm}^{-1}$  bands are assigned to CO stretching of the three CO ligands bound to the fourth Co atom of  $\text{Co}_4(\text{CO})_{12}$ . The 1816  $\text{cm}^{-1}$  band corresponds to the stretching of three edge-bridging CO ligands, each bound to two Co atoms. The stretching frequency of the bridging CO bands  $\nu_{\text{CO}_b}$  is red shifted by about 54  $\text{cm}^{-1}$ , while the terminal CO bands  $\nu_{\text{CO}_t}$  is blue shifted by 18  $\text{cm}^{-1}$  with respect to those of crystalline  $\text{Co}_4(\text{CO})_{12}$ <sup>21</sup> or crystalline  $\text{Co}_4(\text{CO})_{12}$  deposited on the NaY wafer from pentane solution.

**Precursor characterization by EXAFS spectroscopy.** To obtain more insight into the structure of cobalt carbonyl clusters in the precursor, especially into the metal framework, the EXAFS spectra of the Co K edge were analysed. The normalized EXAFS function for the precursor was obtained from the average of X-ray absorption spectra from two scans by a cubic spline background subtraction. The EXAFS function was normalized by division by the height of the absorption edge. The raw EXAFS data of the precursor [Fig. 3(a)] shows oscillations up to a value of  $k$ , the wavevector, of about 12.5  $\text{\AA}^{-1}$ , indicating the presence of near-neighbour high-atomic-weight backscatters, which are inferred to be Co. Since the IR spectra indicate that carbonyl ligands were also present in the precursor, the data were analysed for Co–Co and Co–CO interactions. The raw EXAFS data were Fourier transformed with a  $k^2$ -weighting over the range  $2.0 < k < 16.0 \text{\AA}^{-1}$ . Fig. 3(b) exhibits peaks in the range  $1.3 < R < 2.8 \text{\AA}$  (where  $R$  is the distance from the absorber Co atom), attributable to Co–Co, Co–C and Co(–C–)O contributions. The Fourier-transformed data were then inverse transformed in the range  $1.3 < R < 2.8 \text{\AA}$ , to isolate the major contribution from low-frequency and higher shell contributions. The results of the curve-fitting analyses are shown in Fig. 3(c) and Table 1. The EXAFS results provide the strongest evidence that the backscatters in the immediate vicinity of the Co absorber atoms include Co and low-atomic-weight backscatters, identified as C and O. The relative contributions of these backscattering atoms support the identification of the NaY-encapsulated species as  $\text{Co}_4(\text{CO})_{12}$  for the precursor. All the Co atoms in crystalline  $\text{Co}_4(\text{CO})_{12}$  are stereochemically equivalent, with each bonded to three Co atoms at an average distance of 2.50

$\text{\AA}$ , to 2.63 carbon ligands at an average Co–C distance of 1.84  $\text{\AA}$  and to 2.50 oxygen ligands at an average Co(–C–)O distance of 2.90  $\text{\AA}$  [crystalline  $\text{Co}_4(\text{CO})_{12}$  in Table 1]. The EXAFS results characterizing the precursor were in fair agreement with the crystallographic data for  $\text{Co}_4(\text{CO})_{12}$  (Table 1). The data indicated a Co–Co coordination number of 2.6 with an average Co–Co distance of 2.52  $\text{\AA}$ , a Co–C coordination number of 2.62 with an average Co–C distance of 1.80  $\text{\AA}$  and Co(–C–)O coordination number of 2.54 with an average Co(–C–)O distance of 2.92  $\text{\AA}$  for the sample. On the other hand, the discrepancy between the Co–Co coordination numbers of the precursor and crystalline  $\text{Co}_4(\text{CO})_{12}$  with an  $N(\text{Co–Co})$  ratio of 2.6 : 3.0, implies that about 90% of the Co atoms are present as  $\text{Co}_4(\text{CO})_{12}$  clusters and about 10% of the Co atoms are present as mononuclear forms, such as  $\text{Co}(\text{CO})_4$  species, in the precursor. The calculation of the coordination number for the precursor was in agreement with the abundance of  $\text{Co}_4(\text{CO})_{12}$  and  $\text{Co}(\text{CO})_4^-$  species calculated from the IR peak areas.

**IR and diffuse reflectance results characterizing the decarbonylated cobalt clusters.** When the precursor wafer in the IR cell was exposed to 200 Torr  $\text{O}_2$  at 298–313 K, more dramatic effects were observed: the 1904  $\text{cm}^{-1}$  band disappeared rapidly, while the  $\text{Co}_4(\text{CO})_{12}$  bands at 2078, 2053 and 1816  $\text{cm}^{-1}$  were slightly diminished and the bridging band at 1816  $\text{cm}^{-1}$  shifted down slightly [Fig. 4A(b), (c)]. As the temperature reached 343 K, the bridging CO band at 1816  $\text{cm}^{-1}$  and the terminal CO band at 2053  $\text{cm}^{-1}$  completely disappeared, while the terminal CO band at 2078  $\text{cm}^{-1}$  decreased gradually in intensity [Fig. 4A(e)]. This indicated that some CO ligands of the cobalt clusters vanished and the framework of the cobalt cluster decomposed. Upon raising the temperature to 353 K, the residual CO band eventually disappeared and the clusters were converted to cobalt oxide species [Fig. 4A(f)]. The temperature-programmed oxidation of the precursor was accompanied by the evolution of  $\text{CO}_2$ , and its intense feature at 2354  $\text{cm}^{-1}$  was observed.

As mentioned above, the precursor was stepwise oxidized in 200 Torr  $\text{O}_2$  at 298, 313, 353, 393, 423 and 473 K for 1 h, to form the oxidized samples denoted as  $[\text{Co}_x]_{T, \text{ox}}/\text{NaY}$ , (where the subscript  $T$  refers to oxidation temperature) which were then analysed by UV spectroscopy. The diffuse reflectance spectrum of  $[\text{Co}_x]_{298, \text{ox}}/\text{NaY}$  [Fig. 4B(b)] shows the absorption band at 375 nm, ascribed to the characteristic tetrahedral structure of  $\text{Co}_4(\text{CO})_{12}$ ,<sup>24,25</sup> still remained, as did that of Fig. 4B(a)]. In Fig. 4B(c), the 375 nm band has shifted down slightly and a new absorption band at 575 nm, due to the  $\text{Co}^{\text{II}}\text{O}$  species,<sup>24</sup> is observed. The spectra of  $[\text{Co}_x]_{353, \text{ox}}/\text{NaY}$ ,

**Table 1** Results of the curve-fitting analysis of Co-edge EXAFS data obtained at 296 K for samples<sup>a</sup>

| sample                                       | Co–Co |                |                        |                     | Co–C |                |                        |                     | Co(–C–)O or Co–O |                |                        |                     |
|--|-------|----------------|------------------------|---------------------|------|----------------|------------------------|---------------------|------------------|----------------|------------------------|---------------------|
|  | $N$   | $R/\text{\AA}$ | $\Delta E_0/\text{eV}$ | $\sigma/\text{\AA}$ | $N$  | $R/\text{\AA}$ | $\Delta E_0/\text{eV}$ | $\sigma/\text{\AA}$ | $N$              | $R/\text{\AA}$ | $\Delta E_0/\text{eV}$ | $\sigma/\text{\AA}$ |
| precursor                                    | 2.6   | 2.52           | –10.87                 | 0.027               | 2.62 | 1.80           | 11.79                  | 0.085               | 2.54             | 2.92           | –6.93                  | 0.064               |
| $[\text{Co}_x]_{353, \text{ox}}/\text{NaY}$  |       |                |                        |                     |      |                |                        |                     | 3.67             | 2.01           | 4.16                   | 0.066               |
| $[\text{Co}_x]_{473, \text{ox}}/\text{NaY}$  | 2.90  | 2.86           | –9.74                  | 0.023               |      |                |                        |                     | 5.02             | 1.90           | 4.13                   | 0.039               |
|  | 2.46  | 3.36           | 13.23                  | 0.034               |      |                |                        |                     |                  |                |                        |                     |
| $[\text{Co}_x]_{353, \text{red}}/\text{NaY}$ | 1.12  | 2.56           | 11.60                  | 0.037               |      |                |                        |                     | 2.82             | 1.89           | 3.06                   | 0.020               |
| $[\text{Co}_x]_{473, \text{red}}/\text{NaY}$ | 8.83  | 2.50           | –0.04                  | 0.029               |      |                |                        |                     |                  |                |                        |                     |
| ref. samples                                 |       |                |                        |                     |      |                |                        |                     |                  |                |                        |                     |
| Co foil                                      | 12    | 2.50           | 0.29                   | 0.020               |      |                |                        |                     |                  |                |                        |                     |
| $\text{Co}_4(\text{CO})_{12}$                | 3.0   | 2.50           | –10.09                 | 0.038               | 2.63 | 1.84           | 12.14                  | 0.075               | 2.50             | 2.90           | –8.32                  | 0.061               |
| $\text{Co}_6(\text{CO})_{16}$                | 3.8   | 2.50           | –2.34                  | 0.079               | 2.80 | 1.82           | 8.98                   | 0.067               | 2.63             | 2.92           | –2.15                  | 0.067               |
| $\text{Co}_3\text{O}_4$                      | 4.0   | 2.85           | –11.67                 | 0.047               |      |                |                        |                     | 5.4              | 1.90           | 11.19                  | 0.051               |
|  | 9.3   | 3.40           | –10.89                 | 0.05                |      |                |                        |                     |                  |                |                        |                     |
| CoO <sup>b</sup>                             |       |                |                        |                     |      |                |                        |                     | 8.0              | 2.13           |                        |                     |

<sup>a</sup>  $N$  = coordination number for absorber–backscatter pair;  $R$  = radial absorber–backscatter distance;  $\sigma$  = Debye–Waller factor and  $\Delta E_0$  = inner potential correction. <sup>b</sup> Ref. 24.

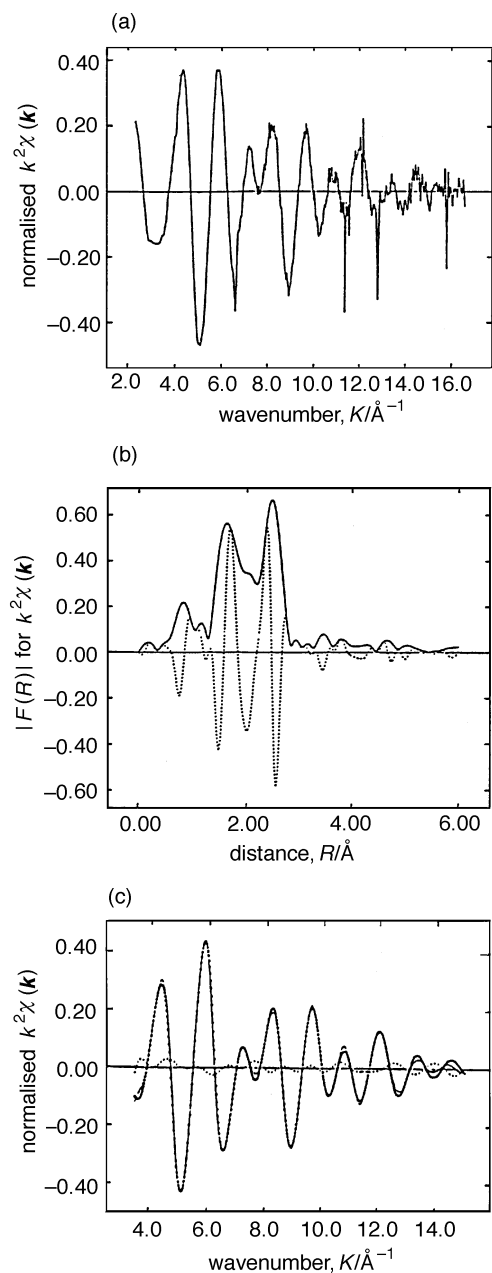


**Fig. 3** Results of EXAFS with the best calculated coordination parameters characterizing the precursor. (a)  $K^2$ -weighted EXAFS spectrum  $K^2\chi(k)$  vs.  $K$ ; (b) Fourier-transform of  $K^2$  weighted EXAFS spectrum  $K^2\chi(k)$  vs.  $R$ . (c) Inverse Fourier-transform of experimental EXAFS in the range  $1.3 < R < 0.28 \text{ \AA}$  (---) and sum of the calculated Co—Co + Co—C + Co(—C—)O contributions (—).

$[\text{Co}_x]_{393, \text{ox}}/\text{NaY}$  and  $[\text{Co}_x]_{423, \text{ox}}/\text{NaY}$  show the absorption band at 375 nm decreases and the band at 575 nm increases with increasing oxidative temperature for the precursor [Fig. 4B(d)–(f)]. In Fig. 4B(g), the spectrum exhibits a dramatic change: the absorption bands at 375 and 575 nm completely disappeared, and the absorption bands at 420 and 700 nm due to  $\text{Co}_3\text{O}_4$  species appeared,<sup>24</sup> indicating that the CoO species converted to  $\text{Co}_3\text{O}_4$  at 473 K. Based on the results of IR and diffuse reflectance, one can safely say that the tetrahedral cobalt clusters species predominate in the sample at a low oxidation temperature, whereas cobalt oxide species predominate in the sample at a high oxidation temperature.

**EXAFS results characterizing the decarbonylated cobalt clusters.** To investigate the structure change of the clusters resulting from a decarbonylated precursor, the oxidized states of the precursor,  $[\text{Co}_x]_{353, \text{ox}}/\text{NaY}$  and  $[\text{Co}_x]_{473, \text{ox}}/\text{NaY}$  were

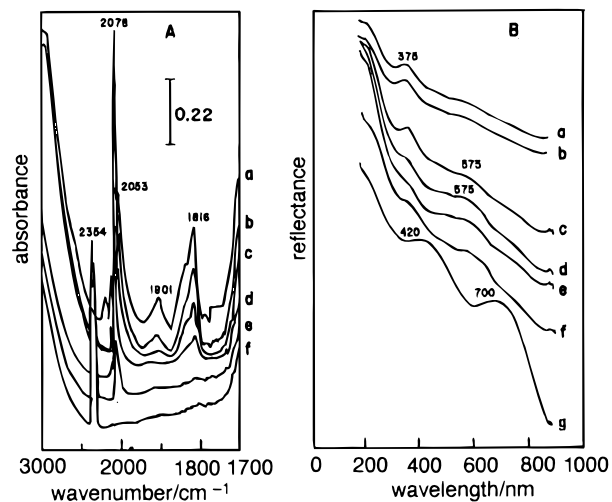


**Fig. 4** A, *In situ* IR spectra characterizing oxidative treatment of the precursor by 200 Torr of  $\text{O}_2$  at 298–353 K: (a) precursor; (b) 298 K, 1 h; (c) 313 K, 1 h; (d) 328 K, 1 h; (e) 343 K, 1 h; (f) 353 K, 1 h. B, Diffuse reflectance spectra characterizing stepwise oxidation of the precursor by 200 Torr of  $\text{O}_2$  at 298–473 K: (a) precursor; (b) 298 K, 1 h; (c) 313 K, 1 h; (d) 353 K, 1 h; (e) 393 K, 1 h; (f) 423 K, 1 h; (g) 473 K, 1 h.

characterized by EXAFS spectroscopy. Fig. 5B1 shows the Fourier-transform function  $K^3\chi(k)$  of  $[\text{Co}_x]_{353, \text{ox}}/\text{NaY}$ . The EXAFS data show the breakage of direct Co—Co bonds and formation of a new species with a Co—O bond at a distance of 2.01 Å, with a coordination number,  $N(\text{Co—O})$ , of 3.67. The Co—O distance is shorter than the 2.13 Å distance observed in crystalline CoO and longer than the Co—O bond (1.90 Å) for crystalline  $\text{Co}_3\text{O}_4$ , as shown in Table 1. A plausible structure for  $[\text{Co}_x]_{353, \text{ox}}$  could be a  $[\text{CoO}]_n$  salt-like structure.<sup>24</sup>

Fig. 5C1 shows the Fourier-transform function  $K^3\chi(k)$  of  $[\text{Co}_x]_{353, \text{red}}/\text{NaY}$ , from  $\text{H}_2$  treatment at a heating rate of 1 K  $\text{min}^{-1}$  to 673 K, followed by 6 h at the final temperature. The EXAFS data show the destruction of the Co—O bond and the formation of Co—Co bonds with a bond length of 2.56 Å. The total  $N(\text{Co—Co} + \text{Co—O})$  of  $[\text{Co}_x]_{353, \text{red}}/\text{NaY}$  is much smaller than those of Co foil or bulk CoO, and even smaller than  $N(\text{Co—Co} + \text{Co—CO})$  of the precursor. This suggests the  $[\text{Co}_x]_{353, \text{red}}/\text{NaY}$  sample retained small cobalt clusters, highly dispersed on the NaY framework. No further aggregation of cobalt clusters was observed even after high-temperature reduction at 773 K. The zeolite channels, with limited sizes, probably prevent cobalt clusters in NaY supercage from coalescing.

### Reaction kinetics and product distribution

Fig. 6 shows temperature-programmed hydrogenation (TPH) spectra of carbonaceous surface species produced by 0.02 mmol  $\text{CH}_4$  dissociation on  $[\text{Co}_x]_{\text{red}}/\text{NaY}$  catalyst at 723 K. The favourable hydrogenation temperature varies with the size of the hydrocarbon. The optimum hydrogenation temperatures of  $\text{C}_2$ ,  $\text{C}_3$ ,  $\text{C}_4$  and  $\text{C}_5$  hydrocarbons were 333, 483, 423 and 453 K, respectively. The  $\text{C}_3$ ,  $\text{C}_4$  and  $\text{C}_5$  hydrocarbon fractions significantly displayed monotonous increases and decreases when  $T$  was set at lower and higher values than their optimum temperature, respectively. The selective catalysis of the reaction is remarkable, with the production of a large amount of  $\text{C}_5$  hydrocarbons but only a trace of  $\text{C}_2$  hydrocarbons at 453 K. At the optimum temperature for each hydrocarbon, the selectivity towards  $\text{C}_2$ ,  $\text{C}_3$ ,  $\text{C}_4$  and  $\text{C}_5$  reached 2.4, 17.7, 11.7 and 46.9%, respectively (Table 2). The range of hydrogenation temperature remarkably affected the yield of the  $\text{C}_{2+}$  hydrocarbons: for  $T = 393$ –543 K,  $\text{C}_{2+}$  selectivity is > 55%; for  $T < 393$  K,  $\text{C}_{2+}$  selectivity reaches 10%, but also non- $\text{C}_4$  and - $\text{C}_5$  species were observed; for

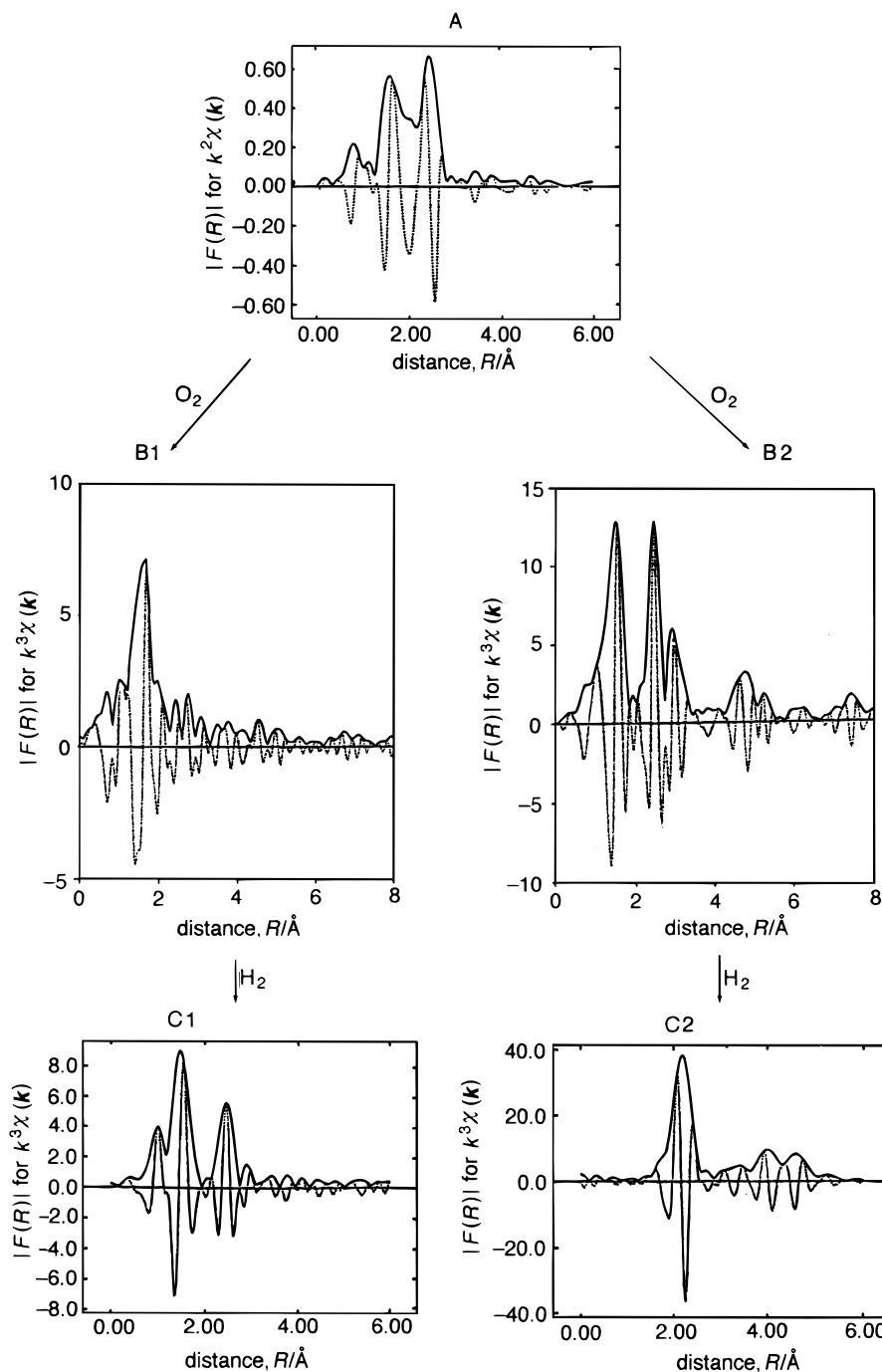


**Fig. 5** Fourier-transform of  $K^3$ -weighted EXAFS spectrum  $K^3\chi(k)$  vs.  $K$  characterizing the sample: A, precursor; B1,  $[\text{Co}_x]_{353,\text{ox}}/\text{NaY}$ ; B2,  $[\text{Co}_x]_{473,\text{ox}}/\text{NaY}$ ; C1,  $[\text{Co}_x]_{353,\text{red}}/\text{NaY}$  from the reduction of  $[\text{Co}_x]_{353,\text{ox}}/\text{NaY}$  at 673 K; C2,  $[\text{Co}_x]_{473,\text{red}}/\text{NaY}$  from the reduction of  $[\text{Co}_x]_{473,\text{ox}}/\text{NaY}$  at 673 K

**Table 2** Kinetic parameters for methane hydrogenation on  $[\text{Co}_x]_{\text{red}}/\text{NaY}$  and  $\text{Co}/\text{SiO}_2$  catalysts<sup>a</sup>

| hydrocarbon    | $[\text{Co}_x]_{\text{red}}/\text{NaY}^b$ |                              | $\text{Co}/\text{SiO}_2^c$ |                              |
|----------------|---|------------------------------|----------------------------|------------------------------|
|                | optimum temp./K                           | selectivity <sup>d</sup> (%) | optimum temp./K            | selectivity <sup>b</sup> (%) |
| C <sub>2</sub> | 333                                       | 2.4                          | 543                        | 3.7                          |
| C <sub>3</sub> | 483                                       | 17.7                         | 543                        | 6.6                          |
| C <sub>4</sub> | 423                                       | 11.7                         | —                          | —                            |
| C <sub>5</sub> | 453                                       | 46.9                         | —                          | —                            |

<sup>a</sup> 100 mg  $[\text{Co}_x]_{\text{red}}/\text{NaY}$  (10 wt.%) or  $\text{Co}/\text{SiO}_2$  (10 wt.%); step 1: exposure of the catalyst to 0.02 mmol  $\text{CH}_4$  at 723 K; step 2: hydrogenation of adspecies by a flow of  $\text{H}_2$  ( $20 \text{ cm}^3 \text{ min}^{-1}$ , 1 atm). <sup>b</sup>  $\text{CH}_4/\text{Co} = 0.11$ . <sup>c</sup>  $\text{CH}_4/\text{Co} = 0.03$ . <sup>d</sup> Molar ratio of  $nC_n$  ( $n = 2, 3, 4$ , or  $5$ )/ $\sum nC_n$  ( $n = 1-5$ ) hydrocarbons.

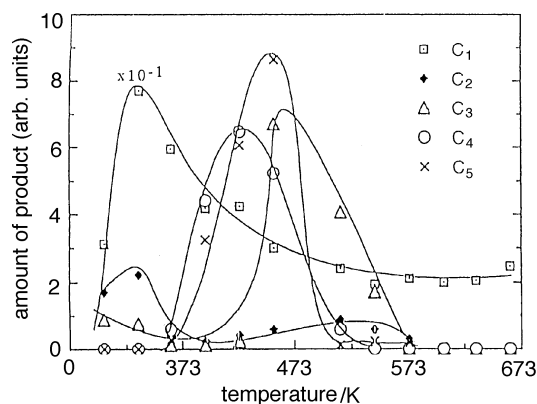


**Fig. 6** Temperature-programmed hydrogenation of the surface carbonaceous species created from 0.02 mmol  $\text{CH}_4$  dissociation on  $[\text{Co}_x]_{\text{red}}/\text{NaY}$  (10% wt. Co) catalyst at 723 K

$T > 543$  K,  $\text{C}_{2+}$  selectivity merely reaches 7%; when  $T$  is increased beyond 673 K, the only product was methane. Moreover, it is interesting that the optimum  $\text{C}_3$  temperature is higher than those of  $\text{C}_4$  and  $\text{C}_5$  (Fig. 6). This implies that a part of  $\text{C}_3$  hydrocarbons would be created by hydrogenolysis of  $\text{C}_4$  and/or  $\text{C}_5$  hydrocarbons.

Fig. 7 shows the hydrocarbon distribution as a function of hydrogenation temperature on the  $\text{Co}/\text{SiO}_2$  catalyst. At an optimum hydrogenation temperature of 543 K, the selectivity of  $\text{C}_2$  and  $\text{C}_3$  only attain 3.7 and 6.6%, respectively (Table 2). The selectivity towards the heavier hydrocarbons ( $\text{C}_4$ ,  $\text{C}_5$ ) was disfavoured even by the same operation on  $[\text{Co}_x]_{\text{red}}/\text{NaY}$ .

Comparison of the kinetic parameters of the reaction between  $[\text{Co}_x]_{\text{red}}/\text{NaY}$  and  $\text{Co}/\text{SiO}_2$  catalysts, summarized in Table 2, shows: (i) the concentration of carbonaceous adspecies on  $[\text{Co}_x]_{\text{red}}/\text{NaY}$  ( $\text{CH}_x/\text{Co}$ , molar ratio) is 3.6 times that on  $\text{Co}/\text{SiO}_2$ , even though an equal amount of methane

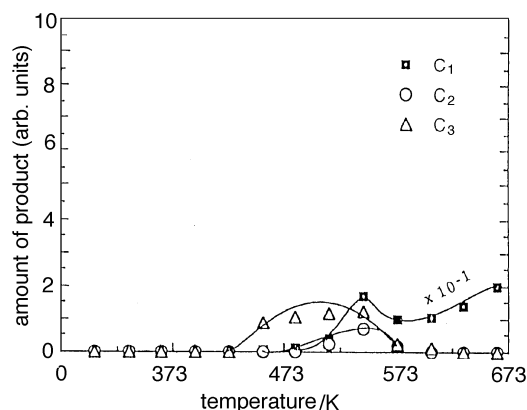


**Fig. 7** Temperature-programmed hydrogenation of the surface carbonaceous species created from 0.02 mmol  $\text{CH}_4$  dissociation on  $\text{Co}/\text{SiO}_2$  (10% wt. Co) catalyst at 723 K

**Table 3** Mode assignments for  $\text{CH}_4$  thermal dissociation on  $[\text{Co}_x]_{\text{red}}/\text{NaY}$  compared to those of ethylene, diazomethane on  $\text{Ru}(001)$  and relevant organometallic complexes (in wavenumbers/ $\text{cm}^{-1}$ )

| mode                 | $\text{CH}_2$ on $\text{Ru}(001)^a$ | $\text{CH}_2$<br>Co—Co | $\text{CH}_2$<br>Os—Os | $\text{CH}_2$<br>Co—Co |
|----------------------|-------------------------------------|------------------------|------------------------|------------------------|
| $\text{CH}_2$ wag    | 1135                                | 1127                   | 961                    | 1393                   |
| $\text{CH}_2$        | 1450                                | 1350                   | 1360                   | 1520                   |
| $\nu_s(\text{CH}_2)$ | 2940                                | 2918                   | 2935                   | 2880                   |
| $\nu_a(\text{CH}_2)$ | 3050                                | 2981                   | 2984                   | 2960                   |
| ref.                 | 26                                  | 26                     | 27 <sup>b</sup>        | this work              |

<sup>a</sup>  $\text{CH}_2$  from both  $\text{C}_2\text{H}_4$  and  $\text{CH}_2\text{N}_2$ .

was exposed to  $[\text{Co}_x]_{\text{red}}/\text{NaY}$  and  $\text{Co}/\text{SiO}_2$ ; (ii) the molar amounts of  $\text{C}_{2+}$  hydrocarbons on  $[\text{Co}_x]_{\text{red}}/\text{NaY}$  catalyst are 10 times those on the  $\text{Co}/\text{SiO}_2$  catalyst; (iii) the hydrocarbon fractions on  $\text{Co}/\text{SiO}_2$  catalyst display a higher desorption temperature than on  $[\text{Co}_x]_{\text{red}}/\text{NaY}$  catalyst. The behaviour of  $[\text{Co}_x]_{\text{red}}/\text{NaY}$  shows that the selectivity towards the heavier hydrocarbons was favoured by  $\text{CH}_4$  thermal dissociation and subsequent hydrogenation at 393–543 K.

### Characterization of carbonaceous adspecies by IR spectroscopy

An IR wafer of  $[\text{Co}_x]_{\text{red}}/\text{NaY}$  was briefly exposed to a flow of  $20 \text{ cm}^{-3} \text{ min}^{-1}$  of dilute  $\text{CH}_4$  (5%  $\text{CH}_4$  in He) at higher temperature, quickly cooled to 298 K and the *in situ* IR spectra recorded. As shown in Fig. 8(A), the weak and medium bands observed at 2960, 2880, 1520 and 1393  $\text{cm}^{-1}$ , respectively, are due to  $\text{CH}_4$  dissociation at 473 K. Georg *et al.* reported the analogous IR frequencies for ethylene and diazomethane thermal chemisorption on an  $\text{Ru}(001)$  surface,<sup>26</sup> and acetylene thermal chemisorption on  $\text{W}(110)$ <sup>26</sup> and  $\text{Ni}(111)$  sur-

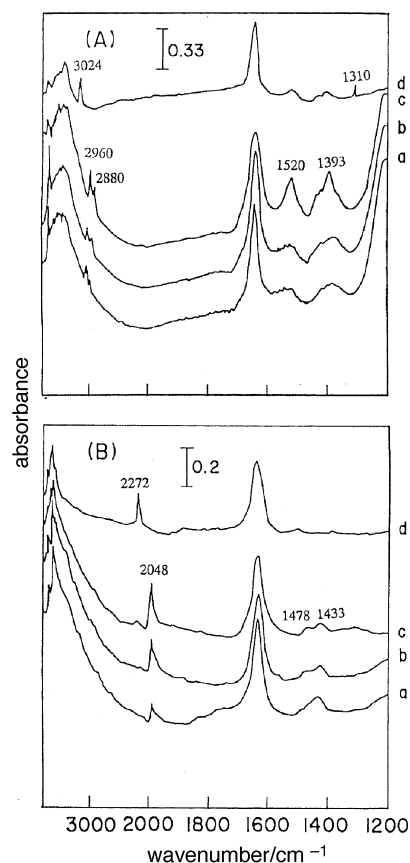


**Fig. 8** *In situ* IR spectra of  $\text{CH}_4$  (A) and  $\text{CD}_4$  (B) dissociation and subsequent hydrogenation or deuteration on  $[\text{Co}_x]_{\text{red}}/\text{NaY}$  catalyst. Decomposition at 473 (a), 573 (b) and 673 K (c); (d) hydrogenation/deuteration at 393 K.

**Table 4** Deuterium distribution in methane obtained from D<sub>2</sub> treatment at 483 K of carbonaceous-deposited material on [Co<sub>x</sub>]<sub>red</sub>/NaY and Co/SiO<sub>2</sub> catalysts

| run | catalyst                               | methane (%)     |                   |                                |                  |                 |
|-----|--|-----------------|-------------------|--------------------------------|------------------|-----------------|
|     |  | CH <sub>4</sub> | CH <sub>3</sub> D | CH <sub>2</sub> D <sub>2</sub> | CHD <sub>3</sub> | CD <sub>4</sub> |
| 1   | [Co <sub>x</sub> ] <sub>red</sub> /NaY | 0               | 0                 | 34.3                           | 40.0             | 25.7            |
| 2   | Co/SiO <sub>2</sub>                    | 0               | 0                 | 0                              | 44.7             | 55.3            |

faces.<sup>27a</sup> Oxtton *et al.*<sup>27b</sup> showed IR bands of the —CH<sub>2</sub> ligand of (μ-CH<sub>2</sub>)[(η-C<sub>5</sub>H<sub>5</sub>)Co(CO)<sub>12</sub>]<sub>2</sub> clusters at 2981, 2918, 1350 and 1127 cm<sup>-1</sup> (Table 3). By comparing IR bands of Fig. 8A(a) with vibrational bands of modes involving the —CH<sub>2</sub> ligands (Table 3), one can reasonably suggest that the 2960 and 2880 cm<sup>-1</sup> bands are assigned to C—H stretching of CH<sub>1,2</sub> adspecies and the 1520, 1393 cm<sup>-1</sup> bands arise from the deformation vibration of CH<sub>2</sub> adspecies. Fig. 8A(b), (c) show the same bands of CH<sub>1,2</sub> but a higher band intensity as compared with that in Fig. 8A(a). This implies that the dissociated fragments successively increased with increasing temperature. As H<sub>2</sub> was admitted into the IR cell with heating, the bands of the CH<sub>x</sub> adspecies disappeared, and new bands at 3024, 1310 cm<sup>-1</sup> appeared, ascribed to physisorption of gaseous CH<sub>4</sub> [Fig. 8A(d)].

In an attempt to confirm that the carbonaceous species was created from CH<sub>4</sub> decomposition, the *in situ* IR spectra of CD<sub>4</sub> thermally dissociated on [Co<sub>x</sub>]<sub>red</sub>/NaY was recorded. Fig. 8B(a) shows C—D stretching and C—D<sub>2</sub> deformation bands at 2048 and 1478, 1433 cm<sup>-1</sup>, respectively. CD<sub>2</sub> and CD species cause overlapping of the C—D stretching vibration at 2048 cm<sup>-1</sup>.<sup>27a,28</sup> The intensity of these bands increased with temperature of CD<sub>4</sub> decomposition [Fig. 8B(a), (c)]. When CD<sub>x</sub> adspecies were treated with deuterium at 393 K, the bands at 2048, 1478 and 1433 cm<sup>-1</sup> disappeared, and a new band emerged at 2272 cm<sup>-1</sup>, assigned to CD<sub>4</sub> physisorption and created from the reaction of CD<sub>x</sub> with D<sub>2</sub>.

By contrast, using the same procedure of CH<sub>4</sub> and CD<sub>4</sub> decomposition on the Co/SiO<sub>2</sub> catalyst led to no carbonaceous species being determined by IR spectra.

### Characterization of carbonaceous adspecies by mass spectrometry

As mentioned above, the carbonaceous species were treated with deuterium at 473 K, and the methane produced was analysed by mass spectrometry (AQ-200, Anelva Co). Run 1 of Table 4 clearly shows the presence of CD<sub>4</sub> (26%), CHD<sub>3</sub> (40%) and CH<sub>2</sub>D<sub>2</sub> (34%). This suggests carbonaceous species such as CH<sub>2</sub>, CH and carbidic carbon were adsorbed on [Co<sub>x</sub>]<sub>red</sub>/NaY.

Run 2 of Table 4 shows only CH (44.7%) and carbidic carbon (55.3%) fragments were deposited on the Co/SiO<sub>2</sub> catalyst. From comparison of runs 1 and 2, it can be assumed that CH<sub>2</sub> adspecies are characteristic of CH<sub>4</sub> thermally decomposed on the [Co<sub>x</sub>]<sub>red</sub>/NaY catalyst which tends to propagate higher hydrocarbons. These differences of the carbonaceous adspecies on [Co<sub>x</sub>]<sub>red</sub>/NaY and Co/SiO<sub>2</sub> catalysts is responsible for the occurrence of high-molecular-weight hydrocarbons on the former.

## Discussion

### Reaction of cobalt carbonyl clusters in NaY zeolite cages

It has been shown that the supercages of NaX zeolite are sufficiently basic to provide an efficient medium for the synthesis of anionic cobalt carbonyl clusters, such as Co(CO)<sub>4</sub><sup>-</sup>.<sup>23</sup> The chemistry of anionic cobalt carbonyl clusters in the cages of NaX zeolite parallels its chemistry in basic solution. On the

weakly basic γ-Al<sub>2</sub>O<sub>3</sub> surface, however, the chemistry of metal carbonyls differs, being similar to that occurring in Lewis-base solution. For example, Co<sub>2</sub>(CO)<sub>8</sub> reacts on the γ-Al<sub>2</sub>O<sub>3</sub> surface to give Co<sub>4</sub>(CO)<sub>12</sub>.<sup>24</sup> The formation of neutral cobalt carbonyl clusters reported here in the NaY zeolite is evidently similar to that occurring on the surface of γ-Al<sub>2</sub>O<sub>3</sub>. Some anionic cobalt carbonyl clusters would be oxidized to neutral cobalt carbonyl clusters by Lewis-acid sites, such as Na<sup>+</sup> or Al<sup>3+</sup> of the NaY zeolite; similarly anionic metal clusters were oxidized by oxidizing agents such as FeCl<sub>3</sub>.<sup>29</sup> The result is not surprising because NaY zeolite is less basic than NaX zeolite. These results give an indication of the possibilities for modification of the reactivity in the solvent-like cages of the zeolites by changing the Si:Al ratio.

The shifts of the terminal and bridging CO bands observed in Co<sub>4</sub>(CO)<sub>12</sub> of the precursor are similar to the shifts observed for metal carbonyls in solutions containing Lewis acids such as Al(C<sub>2</sub>H<sub>5</sub>)<sub>3</sub>, which have been examined extensively.<sup>30</sup> Similar shifts have also been observed for [Rh<sub>6</sub>(CO)<sub>16</sub>] in NaY zeolite and attributed to the interaction of the oxygen atoms of the face-bridging CO ligands with the Lewis-acid sites (Al<sup>3+</sup> ions).<sup>9c</sup> The basicity of the oxygen in CO ligands of metal clusters depends on the CO coordination geometry,<sup>31</sup> as doubly bridging CO ligands are significantly more basic than terminal CO ligands. This pattern is borne out in the present results. The relatively large shift characteristic of the bridging CO band of NaY-supported Co<sub>4</sub>(CO)<sub>12</sub> suggests a strong interaction of the oxygen in bridging CO ligands of the Co<sub>4</sub>(CO)<sub>12</sub> mainly with Na<sup>+</sup> and with possible Lewis-acid sites (Al<sup>3+</sup> ions) formed by dehydration of NaY. Such an interaction is expected to result in a net electron withdrawal from the clusters, decreasing the back-bonding to the terminal CO ligands, strengthening the carbon–oxygen bond, and shifting the terminal CO bands to higher frequencies.

One of the main issues complicating the synthesis and characterization of metal clusters in zeolites is the possible simultaneous formation of metal clusters or crystallites on the external surface of the zeolite. However, the results of the work here suggest that virtually all the cobalt carbonyl clusters were formed in and confined to the NaY cages. When organometallic species from the sample were extracted by methanol solution, the supernatant solution remained colourless and showed no IR absorption in the CO stretching region. These results are consistent with a ‘ship-in-a-bottle’ synthesis of the cobalt carbonyl clusters: the precursor Co<sub>2</sub>(CO)<sub>8</sub> and mobile nucleophilic Co(CO)<sub>4</sub><sup>-</sup> are presumed to be small enough to fit into the interior of the cages; the charged environment, resulting from the large number of Na<sup>+</sup> cations of α-cages,<sup>32</sup> stabilizes the Co(CO)<sub>4</sub><sup>-</sup> within the α-cages; synthetic clusters, Co<sub>4</sub>(CO)<sub>12</sub> are small enough to fit in the supercages of NaY but too large to diffuse rapidly through the apertures. Therefore, Co<sub>4</sub>(CO)<sub>12</sub> clusters, once formed, appear to be encapsulated in the α-cages.

### Decarbonylation of intrazeolitic cobalt carbonyl clusters

The higher-shell Co—Co neighbours cannot be seen in the EXAFS *r*-space diagram of Fig. 5B1 or C1, which is consistent with the inference that there was no cobalt oxide located on the outside of NaY.<sup>33</sup> This agrees with the claim that mild annealing treatment results in the production of small-size cobalt species inside the NaY cages, based on the NMR characterization of size and location of cobalt clusters in NaY by Sachtler and co-workers.<sup>34</sup>

In contrast, the Fourier transform function  $K^3\chi(k)$  of [Co<sub>x</sub>]<sub>473,ox</sub>/NaY from the oxidation of the precursor at 473 K, resembles that of Co<sub>3</sub>O<sub>4</sub> according to the similarity of EXAFS characterization for a Co—O bond at a distance of 1.90 Å (coordination number of 5.02), a Co—Co bond at a

distance of 2.86 Å ( $N = 2.90$ ) and 3.36 Å ( $N = 2.46$ ), as shown in Fig. 5B2 and Table 1. However, the much smaller coordination numbers for Co—Co bonds of the  $[\text{Co}_x]_{473, \text{ox}}/\text{NaY}$ , are in contrast with those of bulk spinel  $\text{Co}_3\text{O}_4$  (Table 1). This indicates a raft-like structure for  $[\text{Co}_3\text{O}_4]_n$  on NaY.<sup>24</sup>

Upon comparison of  $[\text{Co}_x]_{473, \text{red}}/\text{NaY}$  with  $[\text{Co}_x]_{353, \text{red}}/\text{NaY}$  species, the Co—Co coordination number  $N = 8.83$  for the former (Fig. 5C1 and Table 1) is larger than  $N = 1.12$  for the latter (Fig. 5C2 and Table 1). This is an indication of the formation of cobalt particles larger than those of  $[\text{Co}_x]_{353, \text{red}}/\text{NaY}$ . Moreover, the significant peaks at  $r$ -space of 3.9 and 4.7 Å of the Fourier transforms function (Fig. 5C2), corresponding to higher-shell Co—Co neighbours, is evidence of the formation of large cobalt particles, possibly on the external surface. However, EXAFS evidence is lacking for any higher-shell Co atom in  $[\text{Co}_x]_{473, \text{red}}/\text{NaY}$  sample, which is likely a consequence of the limited sensitivity of the EXAFS technique.<sup>35</sup>

The  $[\text{Co}_x]_{353, \text{ox}}/\text{NaY}$  species obtained from mild oxidation of the precursor was very difficult to completely reduce using the same reduction conditions as for  $[\text{Co}_x]_{473, \text{ox}}/\text{NaY}$ , even at 773 K, as evident from its Co—O coordination number of 2.82 (Table 1).

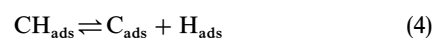
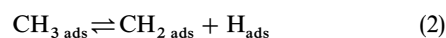
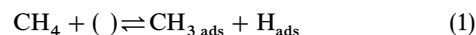
The Co—Co distance characteristic of  $[\text{Co}_x]_{353, \text{red}}/\text{NaY}$  is 2.56 Å, 2% longer than that in Co foil and 1.5% longer than that in the precursor. Tzou *et al.*<sup>36</sup> reported that the Rh—Rh bond of reduced Rh/NaY was about 1–2% shorter than that in Rh foil. Since the Co sample was reduced incompletely, the bonding of O—Co may relax the Co—Co bond.

Thus, one can conclude that the successively decarbonylated sample containing small cobalt clusters, depends on the temperature-programmed oxidation of cobalt carbonyl clusters: mild oxidation caused high dispersion of cobalt oxide, which led to incomplete reduction, while high-temperature oxidation caused larger clusters  $[\text{Co}_3\text{O}_4]_n$  on NaY, allowing easy reduction. The  $\text{Co}_4(\text{CO})_{12}$  was converted to  $[\text{Co}_3\text{O}_4]_n$  species through  $[\text{CoO}]_n$  species *via* a stepwise oxidation process.

In order to ascertain the state of cobalt clusters in NaY cages in the successively decarbonylated precursor, we exposed  $[\text{Co}_x]_{353, \text{ox}}/\text{NaY}$  to NO at 298 K. After 20 min, IR bands at 1894 and 1814  $\text{cm}^{-1}$  appeared and are ascribed, respectively, to the characteristic N—O<sup>δ+</sup> antisymmetrical and symmetrical stretches of  $[\text{Co}^{\text{II}}(\text{NO})_2]$  (not shown). It was interesting to find that the IR spectrum upon NO chemisorption on  $[\text{Co}_x]_{353, \text{ox}}/\text{NaY}$  exhibits significant differences from that on a Co<sup>II</sup>Y sample prepared by ion exchange,<sup>37</sup> apparent from the 20  $\text{cm}^{-1}$  red shift of the N—O band and by the comparison of ON—Co—NO bond angles.<sup>38</sup> Naccache *et al.*<sup>39</sup> suggested that it is possible to distinguish between nitrosyl complexes located in small cavities and those located in large cavities by following the relative rates of reaction between the complexed nitric oxide and molecular oxygen. It is generally believed that NO is able to enter the sodalite cages ( $\beta$ -cages) at 298 K, but that O<sub>2</sub> is not. In order to employ this potentially diagnostic technique, the  $[\text{Co}^{\text{II}}(\text{NO})_2]_{353, \text{ox}}/\text{NaY}$  was exposed to O<sub>2</sub> at 298 K and the pair of NO bands of  $[\text{Co}^{\text{II}}(\text{NO})_2]_{353, \text{ox}}/\text{NaY}$  at 1814 and 1894  $\text{cm}^{-1}$  rapidly decreased, suggesting the  $[\text{Co}_x]_{353, \text{ox}}$  clusters were still located in the  $\alpha$ -cages of NaY, as  $\text{Co}_4(\text{CO})_{12}$ .

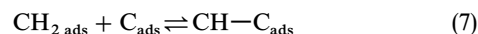
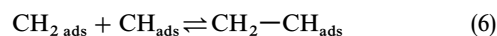
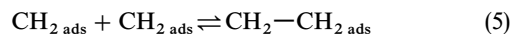
### Procedure for catalysis of methane hydrogenation

An important aspect of our procedure is that the  $[\text{Co}_x]_{\text{red}}/\text{NaY}$  was exposed to flowing  $\text{CH}_4$ -He, so that H<sub>2</sub> produced was continuously removed from the surface. This increased the total amount of adsorbed and its hydrogen deficiency. Based on  $\text{CH}_x$  adspecies determined by IR and mass spectra, one may propose that the processes following  $\text{CH}_4$  chemisorption consists of the stepwise dehydrogenation of  $\text{CH}_x$  groups:



This mechanism indicates that the thermal decomposition of methane on  $[\text{Co}_x]_{\text{red}}/\text{NaY}$  results in H and CH<sub>3</sub> adsorbed on the cobalt surface. Re-dissociation of the CH<sub>3</sub> species into H and methylene can then follow.

The bonding between adjacent hydrogen-deficient  $\text{CH}_x$  groups and growing hydrocarbons chains are reasonably assumed to explain our procedure according to:



and so on. The  $[\text{CH}_x]_{2+}$  surface film was originated on the surface of Co clusters. The  $[\text{CH}_x]_{2+}$  is expected to be similar to those obtained by chemisorption of unsaturated hydrocarbons. Spontaneous desorption of unsaturated hydrocarbons is not favoured in the temperature range that we have explored here and over-heating could cause undesired cracking and coking. In our procedure, flushing with H<sub>2</sub> is the simplest way to release the  $[\text{CH}_x]_{2+}$  unsaturated molecules. However, hydrogenolysis and inter-conversion of the oligomers may unfortunately interfere with the hydrogenation. Occurrence of these competing reaction would explain why the optimum temperature for C<sub>3</sub> is higher than those of C<sub>4</sub> and C<sub>5</sub> hydrocarbons (Fig. 6).

As observed by Feibelman,<sup>40</sup> the adsorption energy of carbon fragments decreases with increasing d-valence occupation. Yang *et al.*<sup>41</sup> calculated that bond energies of CH<sub>3</sub>, CH<sub>2</sub> and CH adsorbed on a Ni(111) surface are 1.7, 2.9 and 3.1 eV, respectively. A similar relative increase of bond energy of  $\text{CH}_x$  ( $x = 0, 1, 2$ ) adspecies on  $[\text{Co}_x]_{\text{red}}/\text{NaY}$  is reasonably expected. Highly hydrogenated  $\text{CH}_x$  ( $x = 2$ ) fragments are thought to be mobile due to the decrease of metal—CH<sub>x</sub> interaction.<sup>30</sup> Therefore, the selectivity to heavier hydrocarbons on  $[\text{Co}_x]_{\text{red}}/\text{NaY}$  is proposed to be due to CH<sub>2</sub> adspecies having a relatively low cobalt—carbon reactivity, being more mobile and more combinative to additional  $\text{CH}_x$  groups. This enhances the chain-growth probability. In contrast, the distribution of C<sub>2</sub> and C<sub>3</sub> lighter hydrocarbons on Co/SiO<sub>2</sub> is ascribed to the lower mobility of carbidic carbon and CH fragments.

The combination of the catalysis of cobalt clusters with steric constraints imposed by the NaY zeolite structure carries great potential for activity and selectivity of methane hydrogenation. The cages allow  $\text{CH}_x$  species to migrate on the surface of the cobalt clusters but without diffusion, owing to the constraints of the zeolite channels. On the other hand, cobalt clusters inside supercages retain a small cluster size, which results in the small  $[\text{CH}_x]_{2+}$  size, as the precursors to the desired C<sub>2+</sub> hydrocarbons. Such control of  $[\text{CH}_x]_{2+}$  film size would greatly reduce the formation of coke.

Based on the determination of carbonaceous adspecies and the kinetic analyses, the reaction mechanism is most likely to consist of: (i) dissociative chemisorption of CH<sub>4</sub>, accompanied by H<sub>2</sub> release, (ii) C—C bond formation and growth of hydrocarbon chains and (iii) subsequent hydrogenation of  $[\text{CH}_x]_{2+}$  film on the cobalt catalyst. Step 2 seems to be the rate determining step.

### Conclusions

NaY-encapsulated  $\text{Co}_4(\text{CO})_{12}$  clusters were synthesized by the adsorption of  $\text{Co}_2(\text{CO})_8$  onto dehydrated NaY under an N<sub>2</sub> atmosphere. The clusters and their decarbonylated products

have been structurally characterized by *in situ* IR, EXAFS, diffuse reflectance spectroscopies and NO chemisorption. EXAFS coordination numbers showed that the successively decarbonylated sample maintained its small cluster size, which depended on the temperature-programmed oxidation of the precursor.

Methane was converted to heavier hydrocarbons by its chemisorption on supported cobalt catalysts and subsequent hydrogenation. NaY-encapsulated Co clusters showed a higher activity and selectivity of C<sub>2+</sub> hydrocarbons, in comparison with a Co/SiO<sub>2</sub> catalyst. The IR and mass spectra and the reaction studies proved that CH<sub>x</sub> (x = 0, 1, 2) adspecies were generated by methane thermal dissociation on the [Co<sub>x</sub>]<sub>red</sub>/NaY catalyst. The CH<sub>2</sub> fragment is quite reactive enabling propagation of higher hydrocarbons.

## References

- J. C. Mackie, *Catal. Rev. Sci. Eng.*, 1969, **33**, 169.
- H. Zanthoff and M. Baerns, *Ind. Eng. Chem. Res.*, 1990, **29**, 2.
- G. J. Hutchings, M. S. Scurrell and J. R. Woodhouse, *Chem. Soc. Rev.*, 1989, **18**, 251.
- T. Tashiro, T. Ito and K. Toi, *J. Chem. Soc., Faraday Trans. 1*, 1985, **81**, 2835.
- M. Nakamoea, H. Mitsuhashi and N. Takezawa, *J. Catal.*, 1992, **138**, 572.
- Q. Y. Yang, A. D. Johnson, K. J. Maynard and S. T. Ceyer, *J. Am. Chem. Soc.*, 1989, **111**, 8748.
- T. Koerts and R. A. Van Santen, *J. Chem. Soc., Chem. Commun.*, 1991, 1281.
- (a) J. G. Goodwin, Jr., *J. Mol. Catal.*, 1982, **14**, 259; (b) R. Pierantozzi, E. G. Valagene, A. F. Nordquist and P. Dyer, *J. Mol. Catal.*, 1983, **21**, 189.
- (a) E. Mantovani, N. Palladino and A. Zanobi, *J. Mol. Catal.*, 1977/1978, **3**, 285; (b) P. Gelin, Y. Ben. Taarit and C. Naccache, *J. Catal.*, 1979, **59**, 537; (c) L-F. Rao, A. Fukuoka, N. Kosugi, H. Kuroda and M. Ichikawa, *J. Phys. Chem.*, 1990, **94**, 5317.
- (a) L. L. Sheu, H. Knözinger and W. M. H. Sachtler, *Catal. Lett.*, 1989, **2**, 129; (b) L. L. Sheu, H. Knözinger and W. M. H. Sachtler, *J. Mol. Catal.*, 1989, **57**, 61; (c) L. L. Sheu, H. Knözinger and W. M. H. Sachtler, *J. Am. Chem. Soc.*, 1989, **111**, 8125.
- (a) S. Kawi and B. C. Gates, *J. Chem. Soc., Chem. Commun.*, 1991, 994; (b) S. Kawi, J-R. Chang and B. C. Gates, *J. Catal.*, 1993, **142**, 585; (c) T. Beutel, S. Kawi, K. Purnell, H. Knözinger and B. C. Gates, *J. Phys. Chem.*, 1993, **97**, 7284.
- (a) A. De. Mallmann and D. Barhomeuf, *Catal. Lett.*, 1990, **5**, 293; (b) G-J. Li, T. Fujimoto, A. Fukuoka and M. Ichikawa, *Catal. Lett.*, 1992, **12**, 171.
- A. Fukuoka, L-F. Rao, N. Kozugi and M. Ichikawa, *Appl. Catal.*, 1989, **50**, 295.
- M. Ichikawa, L-F. Rao, T. Ito and A. Fukuoka, *Faraday Discuss., Chem. Soc.*, 1989, **87**, 232.
- F-S. Xio, A. Fukuoka and M. Ichikawa, *J. Catal.*, 1992, **138**, 206.
- P. A. Jacobs, in *Metal Clusters in Catalysis*, ed. B. C. Gates, L. Guzzi and H. Knözinger, Elsevier, Amsterdam, 1986, p. 357.
- G-C. Shen, A-M. Liu, T. Shido and M. Ichikawa, *Top. Catal.*, 1995, **2**, 141.
- J. B. A. D. van Zon, D. C. Koningsberger, H. F. J. van't Blik and D. E. Sayers, *J. Chem. Phys.*, 1985, **12**, 5742.
- N. Kosugi and H. Kuroda, Program EXAFS 2, Research Center for Spectrochemistry, University of Tokyo, 1988.
- Y-C. Xie and Y-Q. Tang, *Adv. Catal.*, 1990, **37**, 1.
- S. Qui, R. Ohnishi and M. Ichicawa, *J. Chem. Soc., Chem. Commun.*, 1992, 1425.
- F. A. Cotton and R. R. Monchamp, *J. Chem. Soc.*, 1960, 1882.
- (a) R. L. Schneider, R. F. Howe and K. L. Watters, *Inorg. Chem.*, 1984, **23**, 4600; (b) M. C. Connaway and B. E. Hanson, *Inorg. Chem.*, 1986, **25**, 1445.
- Y. Iwasawa, M. Yamada, Y. Sato and H. Kuroda, *J. Mol. Catal.*, 1984, **23**, 95.
- R. A. Friedel, I. Wender, S. L. Shufler and H. W. Sternberg, *J. Am. Chem. Soc.*, 1995, **77**, 3951.
- M. P. Georeg, N. R. Avery, W. H. Weinberg and F. N. Tebbe, *J. Am. Chem. Soc.*, 1983, **105**, 1393.
- (a) J. E. Demuth and H. Ibach, *Surf. Sci.*, 1978, **78**, 1238; (b) I. A. Oxtton, D. B. Powell, N. Sheppard, K. Burgess, B. F. G. Johnson and J. Lewis, *J. Chem. Soc., Chem. Commun.*, 1982, 719.
- M. B. Lee, Q. Y. Yang, S. L. Tang and S. T. Ceyer, *J. Chem. Phys.*, 1986, **85**, 1693.
- (a) V. Albano, P. Chini and V. Scatturin, *Chem. Commun.*, 1968, 163; (b) P. Chini, *Chem. Commun.*, 1967, 440.
- D. F. Shriver, *J. Organomet. Chem.*, 1975, **94**, 259.
- H. H. Lamb, B. C. Gates and H. Knözinger, *Angew. Chem., Int. Ed. Engl.*, 1988, **27**, 1127.
- G. A. Ozin, *Materials Chemistry*, ed. L. V. Interrante, L. A. Casper and A. B. Ellis, *Am. Chem. Soc.*, Washington, DC, 1995, pp. 335–371.
- S. Kawi, J-R. Chang and B. C. Gates, *J. Am. Chem. Soc.*, 1993, **115**, 4830.
- Z. Zhang, Y. D. Zhang, W. A. Hines, J. I. Budnick and W. M. H. Sachtler, *J. Am. Chem. Soc.*, 1992, **114**, 4843.
- S. D. Maloney, M. J. Kelley, D. C. Koningsberger and B. C. Gates, *J. Phys. Chem.*, 1991, **95**, 9406.
- M. S. Tzou, B. K. Teo and W. M. H. Sachtler, *Langmuir*, 1986, **3**, 773.
- J. H. Lansford, P. J. Hutta, M. J. Lin and K. A. Windhorst, *Inorg. Chem.*, 1978, **17**, 606.
- K. A. Windhorst and J. H. Lansford, *J. Am. Chem. Soc.*, 1975, **97**, 1407.
- C. Naccache and Y. B. Taarit, *J. Chem. Soc., Faraday Trans. 1*, 1973, **69**, 1475.
- P. J. Feibeman, *J. Phys. Rev. B*, 1982, **26**, 5347.
- H. Yang and J. L. Whitten, *Surf. Sci.*, 1991, **255**, 193.

Paper 6/05124C; Received 23rd July, 1996